Provenance of the Ebenebe Sandstone: Evidence from X-Ray Fluorescence and Paleocurrent Studies

[1]Uchechukwu Stephanie Ezeani., [2]Onyinye, Lisa Eze., *[3]Gordian Chuks Obi., [4]Ositadimma Igwebuike Chiaghanam

[1,3,4]Chukwuemeka Odumegwu Ojukwu University, Anambra State

[2]Enugu State University of Technology, Enugu State

***Corresponding Author**

DOI: https://doi.org/10.51244/IJRSI.2025.12060013

Received: 11 May 2025; Accepted: 23 May 2025; Published: 27 June 2025

ABSTRACT

The Ebenebe Sandstone is the sandy member of the Paleocene Imo Formation. The sand body in Anambra State was subjected to x-ray fluorescence and paleocurrent analyses to establish the nature of the source rock, the paleoclimatic conditions of the source terrain, and the depositional environment. The research is to provide an insight into the Paleocene-Oligocene tectonic history and paleogeography of the Niger delta basin and the implications for the exploration and exploitation of sand and hydrocarbon resources in the region. Ten fresh and representative samples of the Ebenebe Sandstone were collected from Ugwuoba, Ifite-Awka, Isiagu and Ufuma outcrops respectively. The samples were subjected to X-ray Fluorescence analysis to determine the percentage concentrations of SiO_2, TiO_2, Al_2O_3, Fe_2O_3, MgO, Na_2O, CaO, and K_2O. At each location twenty sets of measurements of dips and azimuths of foreset planes of planar cross-beds were also taken for paleocurrent analysis. X-ray fluorescence studies revealed that the Ebenebe Sandstone is a silica-cemented quartz arenite composed of about 90.5% silica, with deleterious amounts of the oxides of aluminum, iron and titanium. Paleocurrent analysis revealed that the clastics were sourced from a pre-existing sedimentary terrain that lies to the east of the present study area. Chemical parameters further indicates that the terrain lies within a passive margin that experienced intense chemical weathering. It can therefore be concluded that the Ebenebe Sandstone was recycled from a pre-existing sedimentary terrain located to the east of the present study area that most probably became emergent as a result of the asymmetrical subsidence of the post-Santonian Anambra basin. These results thus provide new insight into the tectonic history of the Anambra-Niger delta basin complex.

Keywords: Ebenebe Sandstone, X-ray fluorescence, chemical indices, quartz arenite, asymmetrical subsidence, Niger Delta.

INTRODUCTION

The Ebenebe Sandstone is the sandy component of the Paleocene Imo Formation of the Niger Delta (Table 1.1). It is a prominent sandstone deposits in Anambra State that holds great potentials as a source of commercial silica sand (Ezeani, 2025)[1].

Earlier studies have shown that the Ebenebe Sandstone which occurs as a slightly north-south-oriented sand ridge, is encased by the marine shale components of the Imo Formation (Nwajide, 2013[2], Odunze and Obi, 2014[3]; Fig. 1.1). Studies have also shown that the sand is texturally mature, coarse to fine-grained, and transported from its source by an east-west directed fluvial current (Ezeani, 2025)[1], and deposited in a tide-dominated shelf environment (Ekwenye et al.,2014[4]; Ohwona and Okoro, 2022[5]). Paleocurrent analysis by Obi *et al*, (2001)[6], Ekwenye et al. (2014) [4], Odunze and Obi (2014)[3] has revealed that the sand ridge was shaped by a NW-SE oriented longshore currents.

ISSN No. 2321-2705 | DOI: 10.51244/IJRSI |Volume XII Issue VI June 2025

Table 1.1. Correlation of early Cretaceous-Paleogene strata in south-eastern Nigeria (modified after Nwajide, 2013) [2]

AGE			SOUTH-EASTERN NIGERIA	
30 my	Oligocene	PALEOGENE	Ogwashi-Asaba Formation	NIGER DELTA
54.9 my	Eocene		Ameki/Nanka Formation/Nsugbe Sandstone	
65 my	Paleocene		Imo Formation	
			Nsukka Formation	
73 my	Maastrichtian		Ajali Sandstone	ANAMBRA BASIN
			Mamu Formation	
83 my	Campanian		Nkporo/ Oweli Formation/Afikpo Sandstone/Enugu Shale	
87.5 my	Santonian		Erosion/ Non-deposition	
88.5my	Coniacian		Awgu Group (Agbani Sandstone/Awgu Shale)	SOUTHERN BENUE TROUGH
93 my	Turonian		Ezeaku Group)	
100 my	Cenomanian- Albian		Asu River Group	Asu River Gr
	Aptian Barremian		Un-named Units	
119 my	Hauterivian			
Precambrian			Basement Complex	

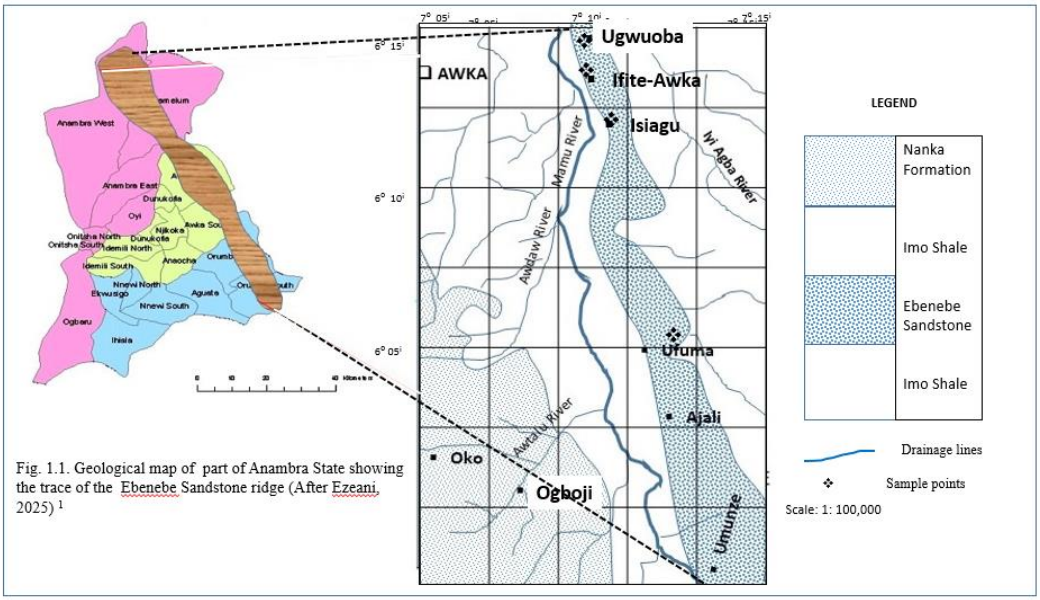

Fig. 1.1. Geological map of part of Anambra State showing the trace of the Ebenebe Sandstone ridge (After Ezeani, 2025) [1]

Apart from these studies, not much is known about the relationship between the post-Maastrichtian tectonic history of the Anambra Basin and provenance of the sandstones in the Anambra-Niger delta basin complex.

The present study aims to interpret the provenance of the Ebenebe Sandstone using x-ray fluorescence method. This method, though less frequently used for the study of sandstone composition, is ideal for the determination of major and minor provenance-sensitive elements such as silicon (Si), aluminium (Al), magnesium (Mg), calcium (Ca), iron (Fe), potassium (K), sodium (Na), titanium (Ti), sulphur (S) and phosphorus (P) (Fairchild, 1988)[7]. The result is expected to provide insight into the Paleocene-Oligocene tectonic history and paleogeography of the Niger delta basin. This will have far reaching implications for the exploration and exploitation of solid minerals and hydrocarbon resources in the region.

Geological Setting

The tectonic history of southeastern Nigeria has been discussed by several workers (e.g. Reyment, 1965[8]; Burke, 1996[9], Murat, 1972[10]; and Benkhelil, 1989[11]). More recent efforts have analyzed the relationship between the pre-Santonian geologic history of the Abakaliki-Benue Trough and tectono-sedimentologic evolution of the post-Santonian Anambra Basin. Prominent among these are the works of Hoque and Nwajide

(1985)[12], Ojoh, (1992)[13], and Obi, *et al*., (2001)[6]. These works have shown that the stratigraphic evolution of the Anambra Basin during the Campanian-Maastrichtian period was controlled by episodic asymmetrical subsidence of the Anambra platform, along the landward extension of the Atlantic Chain fracture associated with the initial opening of the Benue Trough. The subsidence was in response to sediment load and post-Benue rift thermal contraction of the lithosphere (Popoff, 1990)[14], and Binks and Fairhead, 1992)[15].

The Paleogene stratigraphy of south-eastern Nigeria is composed of a general progradational succession that begins with the fluvio-deltaic sandstone, mudstone and thin limestone bands of the Nsukka Formation (Late Maastrichtian-Paleocene; Obi, 2000[16]; Oboh-Ikuenobe et al., 2005[17]). The Nsukka Formation is succeeded by the Imo Formation (Paleocene) consisting of blue-grey clays, shallow marine shale, limestone and calcareous sandstone (Reyment, 1965)[8]. Figure 1.1 shows that in the present study area the mud rock component of the Imo Formation encased the sandstone component called the Ebenebe Sandstone (Oboh-Ikuenobe et al., 2005[17]; Odunze-Akasiugwu and Obi, 2019[18]). According to Nwajide (2013)[2], marine regression during the Eocene led to the accumulation of Ameki Formation and the Nanka Sand.

METHOD OF STUDY

X-ray Fluorescence Study

Ten (10) fresh and representative samples of the Ebenebe Sandstone were collected from Ugwuoba, Ifite-Awka, Isiagu and Ufuma outcrops respectively (Fig. 1.1) and subjected to X-ray Fluorescence analysis to determine the percentage concentrations of SiO_2, TiO_2, Al_2O_3, Fe_2O_3, MgO, Na_2O, CaO, and K_2O. The samples were first crushed to reduce the grains to less than 63 microns using the Tema vibrating mill. About 5.0g of dry rock sample powder was weighed in a silica crucible, and ignited in the furnace at 1000^0c for 2 to 3 hours for the calcinations of impurities in the rock powder. The samples were then allowed to cool to room temperature in desiccators, and then weighed again to determine the weight of calcinated impurities such as H_2O, H_2O^+ and CO_2.

One gram (1.0g) of the rock powder was mixed with X-ray Flux-Type 66:34% (66.0%), Lithium Tetraborate: 34% Lithium metaborate) to lower the vitrification temperature of the rock powder. The weighed mixture was ignited in the pre-set furnace (Eggon 2 Automatic fuse bead maker) at 1500^0c for 10 minutes to form glass bead. Each glass bead was labelled and slotted into the computerized XRF (Epilson 5 Panalytical model) for major elemental analysis.

Paleocurrent Analysis

A total of eighty-two (82) sets of measurements of dips and azimuths of foreset planes of planar cross-beds were measured and subjected to paleocurrent analysis. Twenty (20) sets each were taken from Ugwuoba, Ifite Awka and Isiagu, and twenty-two (22) from Enuguabor-Ufuma (Fig. 1.1). To determine the paleocurrent parameters the azimuth data for each location were first grouped and then plotted as Rose diagrams.

The statistical method described by Steinmetz (1962)[19] was followed to compute the paleocurrent parameters including the *mean vector azimuth R, variance S^2 and the vector strength S*. The computational procedure is illustrated in Table 2.1. Strict attention was paid to the sign of natural trigonometric functions.

Table 2.1. Computational procedure for paleocurrent analysis (After Steinmetz, 1962)[9] A_i stands for individual measurements, D = dip of the cross bed; Sin A and Cos A stand for the sines and cosines of individual azimuths readings; Sin D stands for the sine of the dip angle, *R* is the mean vector azimuth and *n* stands for the total number of readings

Ugwuoba	1	2	3	4	5	6	7	8	9
	Azimuth (A)	Dip (D)	Sin A	Cos A	Cos D	5*4 (b)	5*3 (a)	Sin D (c)	$(A_i-R)^2$
1	304	22	-0.8290	+0.5592	+0.9272	+0.5184	-0.7686	0.3746	104.04
2	360	20	0.0	+1.0000	+0.9397	+0.9397	0	0.3420	2097.64

ISSN No. 2321-2705 | DOI: 10.51244/IJRSI |Volume XII Issue VI June 2025

The validity of columns 6 through 8 was kept in check as suggested by Steinmetz (1962), by means of the identity**:**

$$b^2 + a^2 + c^2 = 1.000 \pm 0.003 \quad (1)$$

The mean vector azimuth, (*R), variance (*S^2*)* and the vector strength (the clustering of the directions about the mean vector azimuth) were determined quantitatively using the following relations given by Steinmetz (1962)[19], Marsal (1987)[20], and Collinson and Thompson, (1989)[21]:

$$Arc\ tan\ R = (\Sigma a) / (\Sigma b) \quad (2)$$

$$S^2 = \Sigma \frac{(A_i - R)^2}{n-1} \quad (3)$$

$$S = \sqrt{\frac{(\Sigma \sin A)^2 + (\Sigma \cos A)^2}{N}} \quad (4)$$

Where A_i stands for individual measurements, D = dip of the cross bed; Sin A and Cos A stand for the sines and cosines of individual azimuths readings; Sin D stands for the sine of the dip angle, ***R*** is the mean vector azimuth and ***n*** stands for the total number of readings.

RESULTS AND INTERPRETATION

Composition: The result of the analysis including the percentages of the raw oxides, and chemical indices of alteration (as defined by Nesbit et al., 1996[22]), and the ratios of the oxides are shown in Table 3.1. The result reveals that quartz (SiO_2) has the highest concentration that ranges from about 89% to approximately 92%, with an average of 90.57%. Next in abundance is Alumina Al_2O_3, (4.15%-6.74%), followed by Iron oxide, Fe_2O_3 (2.44%-3.80%).

Table 3.1.: Result of X-Ray Fluorescence Analysis showing the chemical composition, indices of alteration, and ratios of oxides.

CHEMICAL COMPOSITION	Ugwuoba		Ifite-Awka		Isiagu			Ufuma			AVERAGE
Oxides %	1	2	3	4	5	6	7	8	9	10	
SiO_2	90.63	90.34	88.93	89.39	91.29	92.49	91.29	91.79	89.29	90.29	90.57
TiO_2	0.33	0.25	0.24	0.23	0.15	0.32	0.23	0.18	0.24	0.20	0.24
Al_2O_3	6.52	6.74	6.56	5.10	4.90	4.15	4.50	4.30	5.0	5.2	5.30
Fe_2O_3	2.44	2.59	3.80	3.45	3.35	2.62	3.10	3.22	3.70	3.80	3.21
MgO	0.01	0.01	0.10	0.10	0.05	0.04	0.01	0.01	0.12	0.15	0.06
K_2O	0.01	0.01	0.01	0.01	0.01	0.01	0.01	0.01	0.01	0.01	0.01
Na_2O	0.01	0.01	0.01	0.01	0.01	0.01	0.01	0.01	0.01	0.01	0.01
CaO	0.05	0.05	0.65	1.71	0.25	0.36	0.76	0.49	1.64	0.34	0.63
CHEMICAL INDICES OF ALTERATION	1	2	3	4	5	6	7	8	9	10	AVERAGE
$PIA = Al_2O_3-K_2O)/(Al_2O_3 + CaO^* + Na_2O- K_2O)] \times 100.$	99.086	98.82	90.59	74.52	94.58	91.39	85.04	89.20	88.32	93.34	90.49
$CIA=100*Al_2O_3/(Al_2O_3+CaO+K_2O+Na_2O)]$	98.94	98.97	90.73	74.67	94.78	91.61	85.52	89.40	75.07	93.52	89.32
[MIA = 2*(CIA-50)]	97.88	97.94	81.46	49.34	89.44	83.22	71.04	78.80	50.14	87.04	78.63
RATIOS OF OXIDES	1	2	3	4	5	6	7	8	9	10	AVERAGE
TiO_2/Al_2O_3	0.1375	0.099	0.09375	0.0958	0.0633	0.1488	0.092	0.01	0.096	0.0909	0.093
Fe_2O_3/Al_2O_3	0.31	0.60	0.55	1.02	0.57	0.71	0.58	0.53	0.68	0.82	0.54
MgO/Al_2O_3	0.004	0.004	0.040	0.042	0.21	0.018	0.004	0.004	0.048	0.068	0.044
Na_2O/Al_2O_3	0.020	0.833	0.031	0.025	0.013	0.005	0.004	0.004	0.004	0.005	0.094
K_2O/Al_2O_3	0.354	0.095	0.254	0.086	0.527	0.470	0.224	0.413	0.404	0.227	0.305
(Fe_2O_3/K_2O)	0.870	6.250	2.154	11.666	1.080	1.505	2.590	1.284	1.683	3.600	3.268
K_2O/Na_2O	17.000	1.143	8.125	3.500	41.666	101.00	56.000	95.000	101.000	50.000	47.443
$((Fe_2O_3+MgO)/(Na_2O+K_2O))$	0.8333	3.355	2.055	9.444	1.094	1.529	2.561	1.281	1.784	3.823	2.776
Na_2O/K_2O	0.006	0.875	0.123	0.286	0.024	0.009	0.018	0.011	0.009	0.02	0.138
$Na_2O + K_2O$	0.9	0.45	0.73	0.27	1.28	1.02	0.57	0.96	1.02	0.51	0.771
SiO_2/Al_2O_3	39.471	37.214	36.301	38.912	39.494	43.530	37.316	40.778	36.916	42.545	39.247
Al_2O_3/TiO_2	7.272	10.08	10.667	10.435	15.8	6.719	10.869	10.00	10.417	11.00	10.326
$Al_2O_3 + K_2O + Na_2O$	3.3	2.97	3.29	2.67	3.65	3.17	3.07	3.26	3.52	2.71	3.161
$CaO + Na_2O$	0.92	0.80	0.48	0.49	0.28	0.37	0.77	0.50	1.65	0.55	0.681
$Al_2O_3/ (CaO + Na_2O)$	2.609	3.15	5.333	4.898	8.464	5.811	3.247	4.6	1.515	4	4.363
$MgO + Fe_2O_3$	0.75	1.51	1.50	2.55	1.40	1.56	1.46	1.23	1.82	1.95	1.573

The ratio of silica to alumina (SiO_2/Al_2O_3) varies from about 36% to 43.5%, with an average of 39.2% (Table 3.1). The Table also shows that the average ratio of SiO_2 to Al_2O_3 is high in all samples implying that there is minimal clay or detrital Aluminum Silicate within the Ebenebe Sandstones in the study area. It is also evident that the percentage of total alkali-earth oxides is low, thus suggesting that the Ebenebe Sandstone is dominantly cemented by silica.

ISSN No. 2321-2705 | DOI: 10.51244/IJRSI |Volume XII Issue VI June 2025

Classification: Pettijohn (1963)[23] and Pettijohn *et al.*, (1972)[24] classified sandstones based on their chemical composition. The classification scheme used the log of the ratio of SiO_2 to Al_2O_3 to differentiate mature sandstones high in SiO_2/Al_2O_3 ratios, and immature sandstones high in Na_2O/K_2O ratios (Table 3.2). Four classes are recognized by Pettijohn *et al.*, (1972)[24] namely (i) Arenites with log of SiO_2 to Al_2O_3 ratio greater than 1.5, (ii) greywackes with log of SiO_2 to Al_2O_3 ratio greater than 1.0 and log of K_2O/Na_2O less than zero; (iii) arkose, with log of SiO_2 to Al_2O_3 ratio greater than 1.5 and log of K_2O/Na_2O greater than zero and log $(Fe_2O_3+MgO)/(Na_2O+K_2O)$, and (iv) lithic arenite with log of SiO_2 to Al_2O_3 ratio greater than 1.5, and either log K_2O/Na_2O less than 0 or log $(Fe_2O_3+MgO)/Na_2O$ greater than 0 (Table 3.2).

The log of the silica: alumina ratios computed for the Ebenebe Sandstone (Table 3.3) ranges from 1.56 to 1.64, with an average value of 1.59, but the Na_2O/k_2O ratio is consistently zero. Based on the computed log ratios of the chemical oxides (Table 3.3) and on the classification scheme of Pettijohn *et al.*, (1972[24]; Table 3.2), the Ebenebe Sandstone is classified as silica-cemented quartz arenite.

Table 3.2: Chemical classification sandstone using log ratios (Pettijohn, *et al.*, 1972) [24]

S/N	Log of ratios of oxides	Types of sandstone
1	Log $(SiO_2/Al_2O_3) > 1.5$	Arenite
2	Log $(SiO_2/Al_2O_3) > 1$ and Log $(K_2O/Na_2O) < 0$	Greywacke
3	Log $(SiO_2/Al_2O_3) > 1.5$ and Log $(K_2O/Na_2O) > 0$ and log $(Fe_2O_3 + MgO)/(Na_2O + K_2O)$	Arkose
4	Log $(SiO_2/Al_2O_3) > 1.5$ and either Log $(K_2O/Na_2O) < 0$ and log $(Fe_2O_3 + MgO)/(Na_2O > 0$	Lithic arenite

Table 3.3. Computed logs of the ratios of oxides for the ten samples

Sample	Log (SiO_2/Al_2O_3)	Log $(MgO + Fe_2O_3)$	Log (Fe_2O_3/K_2O)	Log $((Fe_2O_3+MgO)/(Na_2O+K_2O))$	Log (K_2O/Na_2O)	Log $((Fe_2O_3 + MgO)/Na_2O)$
1	1.60	0.39	2.387389	2.09	0.0	2.389166
2	1.57	0.41497	2.41329	2.11394	0.0	2.41497
3	1.56	0.591064	2.579783	2.290034	0.0	2.414973
4	1.59	0.550228	2.537819	2.249798	0.0	2.550228
5	1.64	0.531478	2.525044	2.230448	0.0	2.531478
6	1.64	0.42488	2.418301	2.123851	0.0	2.424881
7	1.57	0.492760	2.491361	2.131939	0.0	2.492760
8	1.61	0.509202	2.507855	2.208172	0.0	2.509202
9	1.57	0.582063	2.568201	2.281033	0.0	2.582063
10	1.63	0.596597	2.579783	2.582063	0.0	2.596970
Average	1.59	0.51	2.579783	2.20	0.0	2.50

Herron (1988)[25] used the plot of log (SiO_2/Al_2O_3) against log (Fe_2O_3/K_2O) to classify sandstones and shales. To confirm the above interpretation we employed the Herron's (1988)[25] plot. The plot of log (SiO_2/Al_2O_3) against log (Fe_2O_3/K_2O) for the Ebenebe Sandstone (Fig. 3.1) confirmed the quartz arenite interpretation.

ISSN No. 2321-2705 | DOI: 10.51244/IJRSI |Volume XII Issue VI June 2025

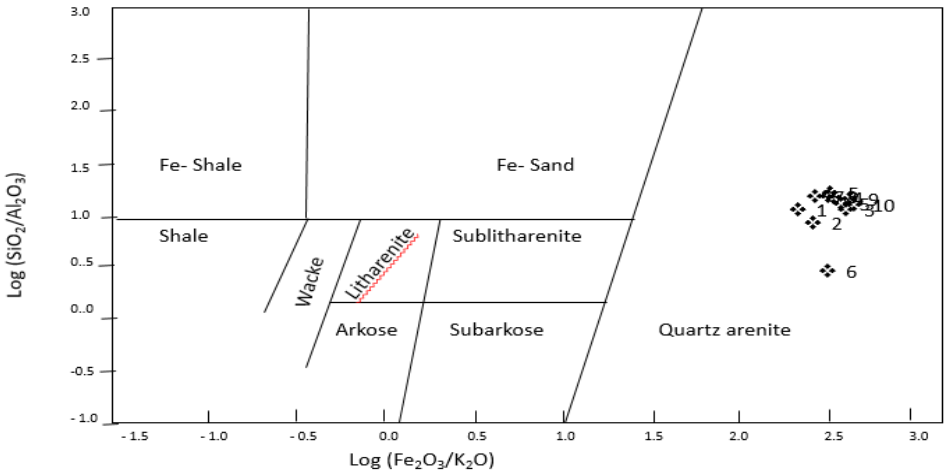

Fig.:3.1. Chemical classification of the Ebenebe Sandstone using binary plot of log (SiO_2/Al_2O_3) against log (Fe_2O_3/K_2O) (Herron, 1988)[25].

Nature of the parent rock:

Roser and Korsch (1988)[26] have demonstrated that the nature of the parent rock of sandstones can be interpreted using discriminant functions based on a plot of the log of the ratio Fe_2O_3/K_2O against log SiO_2/Al_2O_3 .The functions are defined as follows:

Discriminant function-1 (DF-1) =

$[-1.773TiO_2 + 0.607Al_2O_3 + 0.76Fe_2O_3]-[1.5MgO + 0.616CaO + 0.509\ Na_2O - 1.224\ K_2O - 9.09]$

Discriminant function-2 (DF-2) =

$[0.445TiO_2 + 0.07Al_2O_3 - 0.25Fe_2O_3]-[1.42MgO + 0.438CaO + 1.475Na_2O + 1.426\ K_2O - 6.861]$.

The method distinguishes sediment source into four provenance zones: (i) Quartzose sedimentary terrain, (ii) Intermediate igneous terrain, (iii) Felsic igneous rock terrain, and (iv) Mafic igneous terrain.

The nature of the parent rock for the Ebenebe Sandstone was interpreted using the discriminant functions as proposed by Roser and Korsch (1988)[26]. The mathematical computation of the functions is summarized in Table 3.4.

Table 3.4.: Discriminant analyses (DF1 and DF2) for the Eenebe Sandstone using the raw oxides

DF1	$-1.773TiO_2$	$+0.607Al_2O_3$	$+0.76Fe_2O_3$	$-1.5MgO$	$+0.616CaO$	$+0.509Na_2O$	$-1.224K_2O$	-9.09	TOTAL DF-1
1	-0.58509	+ 3.95764	+ 1.8544	- 0.015	0.0308	+ 0.00509	- 0.0122	-9.09	-3.46498
2	-0.44325	+ 4.09118	+ 1.9684	- 0.015	+ 0.0308	+ 0.00509	- 0.0122	- 9.09	-4.67278
3	-0.42552	+ 3.98192	+ 2.888	- 0.15	+ 0.4004	+ 0.00509	- 0.0122	- 9.09	- 3.61011
4	-0.40779	+ 3.0957	+ 2.622	- 0.15	+ 1.05336	+ 0.00509	- 0.0122	- 9.09	- 4.09164
5	- 0.26595	+ 2.9743	+ 2.546	- 0.075	+ 0.154	+ 0.00509	- 0.0122	-9.09	- 4.97156
6	- 0.56736	+ 2.51905	+ 1.9912	- 0.06	+ 0.22176	+ 0.00509	- 0.0122	-9.09	- 5.54406
7	- 0.40779	+ 2.7315	+ 2.356	- 0.015	+ 0.46816	+ 0.00509	- 0.0122	-9.09	- 5.17204
8	-0.31914	+ 2.6101	+ 2.4472	- 0.015	+0.30184	+ 0.00509	- 0.0122	-9.09	- 5.27991
9	-0.42552	+ 3.035	+ 2.812	- 0.18	+ 1.01024	+ 0.00509	- 0.0122	-9.09	-4.05319
10	- 0.3546	+ 3.1564	+ 2.888	- 0.225	+ 0.20944	+ 0.00509	- 0.0122	-9.09	- 4.63067

DF2	$0.445TiO_2$	$+0.07Al_2O_3$	$-0.25Fe_2O_3$	$-1.42MgO$	$+0.438CaO$	$+1.475Na_2O$	$+1.426K_2O$	–6.861.	TOTAL DF-2
1	0.14685	0.4564	-0.61	-0.0142	+0.0219	+0.01475	+0.01426	–6.861.	-6.83104
2	0.11125	0.4718	-0.6475	-0.0142	+0.0219	+0.01475	+0.01426	–6.861.	-6.88874
3	0.1068	0.4592	-0.95	-0.142	+0.2847	+0.01475	+0.01426	–6.861.	-7.07329
4	0.10235	0.357	-0.8625	-0.142	+0.74898	+0.01475	+0.01426	–6.861.	-6.49982
5	0.006675	0.343	-0.8375	-0.071	+0.1095	+0.01475	+0.01426	–6.861.	-7.281315
6	0.1424	0.2905	-0.655	-0.0568	+0.15768	+0.01475	+0.01426	–6.861.	-6.95321
7	0.10235	0.315	-0.775	-0.0142	+0.33288	+0.01475	+0.01426	–6.861.	-6.87096
8	0.0801	0.301	-0.805	-0.0142	+0.21462	+0.01475	+0.01426	–6.861.	-7.05547
9	0.1068	0.350	-0.925	-0.1704	+0.71832	+0.01475	+0.01426	–6.861.	-6.75227
10	0.089	0.364	-0.95	-0.213	+0.14892	+0.01475	+0.01426	–6.861.	-7.39307

Plots of the log of the ratio Fe_2O_3/K_2O against log SiO_2/Al_2O_3 (discriminant functions -1 against discriminant functions -2) using the raw oxides (Fig. 3.2) show that all the samples of the Ebenebe Sandstone analysed in this study plotted within the quartzose sedimentary provenance thus suggesting that the Ebenebe Sandstone clastics were generated from a pre-existing sedimentary terrain

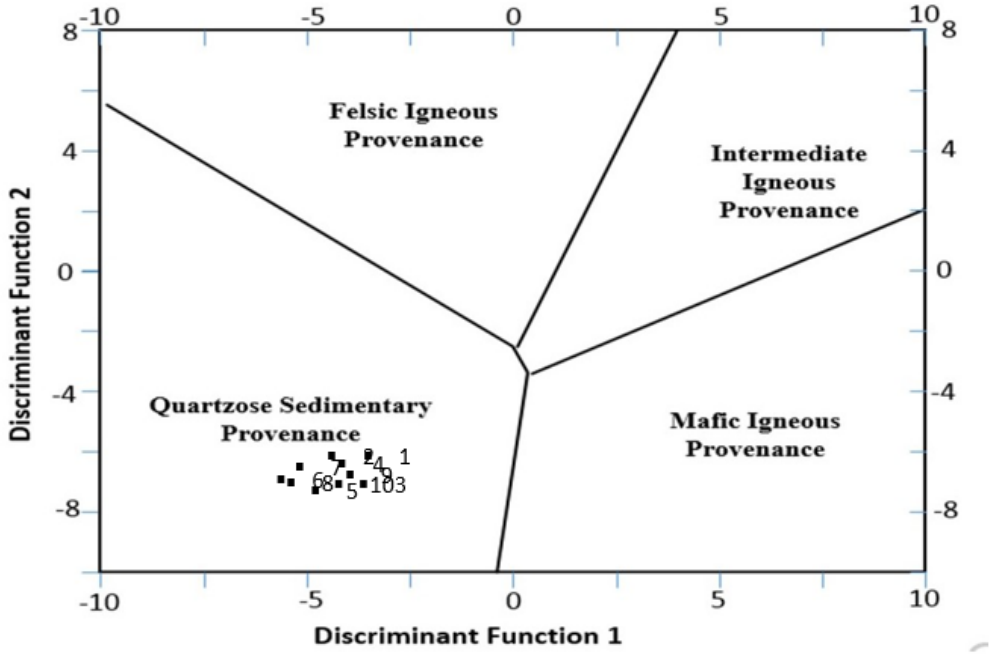

Fig. 3.2.: Discriminant function diagram using raw oxide values (After Roser & Korsch, 1988) [25]

Paleotectonics of the Source Terrain: The use of geochemical parameters in provenance studies has largely focused on interpretation of tectonic setting. Crook (1974)[27] demonstrated that the ratio of SiO_2 and K_2O/Na_2O in sandstone can be employed in provenance studies to distinguish the tectonic setting of sandstones. Crook (1974)[27] used the plot of the log of K_2O/Na_2O against SiO_2 to discriminate oceanic island arc, active continental, and passive margins. This techniques was used in this study to interpret the tectonic setting of the region from where the Ebenebe Sandstone clastics were generated. Figure 3.3 shows that the samples plotted essentially within the passive margin.

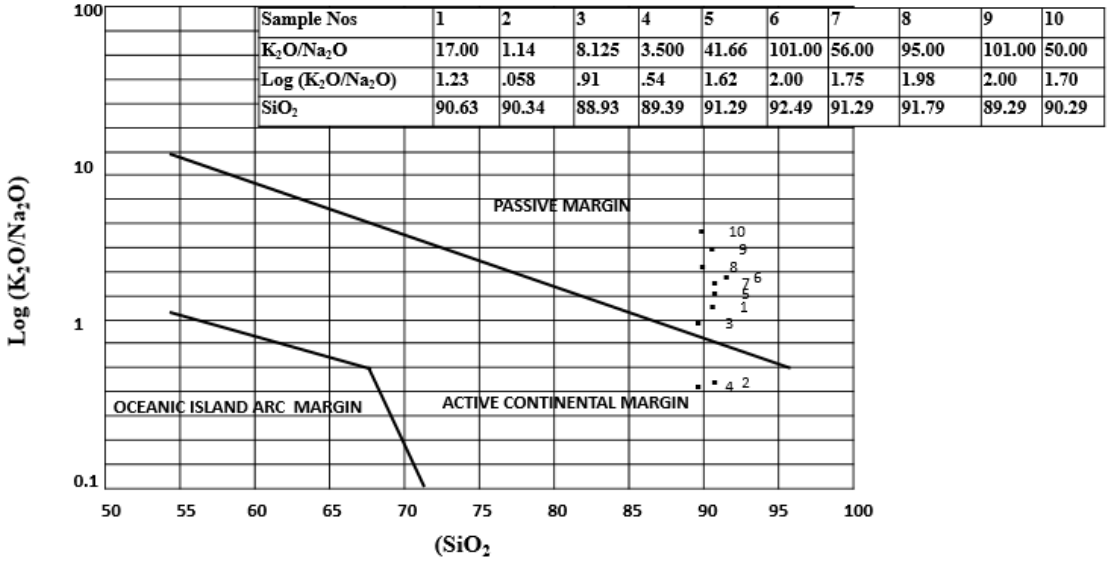

Sample Nos	1	2	3	4	5	6	7	8	9	10
K_2O/Na_2O	17.00	1.14	8.125	3.500	41.66	101.00	56.00	95.00	101.00	50.00
Log (K_2O/Na_2O)	1.23	.058	.91	.54	1.62	2.00	1.75	1.98	2.00	1.70
SiO_2	90.63	90.34	88.93	89.39	91.29	92.49	91.29	91.79	89.29	90.29

Fig. 3.3. A Binary plot of log (K_2O/Na_2O) against SiO_2 (After Crook (1974) [27] discriminating the tectonic setting for the Ebenebe Sandstone.

Source Rock Weathering: Nesbitt et al. (1996)[22] have shown that the chemical composition of clastic sedimentary rocks depends largely on the degree of weathering in the source region. To interpret the degree of

ISSN No. 2321-2705 | DOI: 10.51244/IJRSI |Volume XII Issue VI June 2025

weathering in the Ebenebe Sandstone source region, the Chemical Index of Alteration (CIA) was calculated using the relation: [CIA=100*Al_2O_3/(Al_2O_3+CaO+K_2O+Na_2O)] as suggested by Nesbitt and Young (1982)[28]. The procedure measures the ratio of secondary aluminous minerals to feldspar, hence forms the basis for understanding the weathering intensity on source rocks (Elzien et al., 2014[29]; Mgbenu, 2018[30]; Echefu, 2019[31]). Values of CIA below 50 indicate weak weathering or an un-weathered upper crust while values above 76 suggest intense weathering and/or a total removal of alkali and alkali-earth elements with an enrichment of alumina (Fedo et al., 1995[32]; Dupuis et al., 2006[33]).

The result (Table 3.1) shows that the Ebenebe Sandstone has an average chemical index of alteration of 89.32%. This high value indicates that the source region experienced intense chemical weathering.

Two other indices were also applied to gain more insight into the degree of weathering in the source region. These include the Mineralogical Index of Alteration (MIA) and the Plagioclase Index of Alteration (Harnois, 1988)[34]. The two indices are defined as follows:

(i) Mineralogical Index of Alteration [MIA = 2*(CIA-50)]

(ii) Plagioclase Index of Alteration = [(Al_2O_3-K_2O)/(Al_2O_3 + CaO* + Na_2O- K_2O)] × 100 (where

CaO represents the calcium oxide within the silicate fraction).

MIA values 0%-20% indicate incipient weathering, 20-40% indicate weak weathering, 40-60% indicate moderate weathering, while 60-100% indicate intense to extreme degree of weathering (Harnois, 1988)[34]. The results (Table 3.1) show that MIA values range from 74.67% to 98.94%, giving an average of 78.63%. This confirms that the source region for the Ebenebe Sandstone experienced intense chemical weathering. This interpretation is consistent with the results obtained for the Plagioclase Index of Alteration (PIA). The Plagioclase Index of Alteration (PIA) values obtained in this study (Table 3.1) range from 49.34% to 97.94%, with an average of 90.49%. This further confirms that chemical weathering in the source region was intense.

Results and Interpretation of Paleocurrent Analysis

The grouped paleocurrent data for the Ebenebe Sandstone is presented in Table 3.5, while the Rose diagrams are shown in Figures 3.4 and 3.5. The computational procedure for the analysis of the paleocurrent data from Ugwuoba, Ifite Awka, Isiagu and Enuguabor-Ufuma are displayed in Tables 3.6 -3.9, while the derivation of the paleocurrent parameters is summarized in Table 3.10.

Table 3.5. Grouped paleocurrent data for the Ebenebe Sandstone in the study area

Locality	31-60^0	61-90^0	91-120^0	121-150^0	151-180^0	181-210^0	211-240^0	241-270^0	271-300^0	301-330^0	331-360^0	Total Readings
Ugwuoba	==	==	2	6					5	4	3	20
Ifite Awka	3			1	3	11			2			20
Isiagu						5	8	2	3	2		20
Ufuma					6	1	5	2	3	3	2	22

The following deductions are made from the rose diagrams. and from the computed parameters:

- The Ebenebe Sandstone is characterized by bimodal, often locally radial palaeocurrent pattern that includes south/southwesterly, and northwesterly modes with variance that ranges between 1,800 and 4,600, and a generally high dispersion (vector strength = 0.15 to 0.8) of flow directions about the mean vector azimuths. The mean vector azimuth is consistently westerly to northwesterly (186^o-314^o).

ISSN No. 2321-2705 | DOI: 10.51244/IJRSI |Volume XII Issue VI June 2025

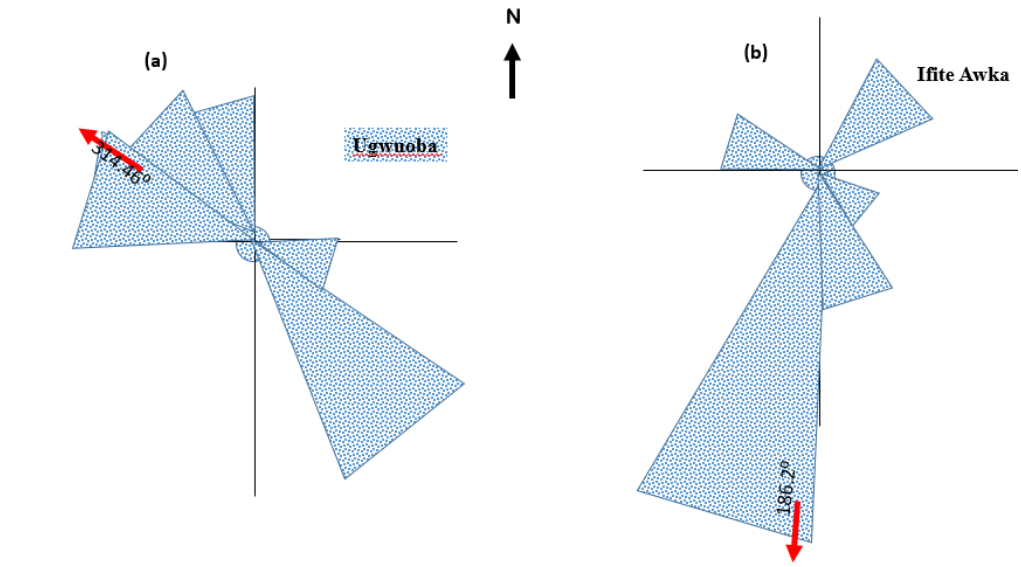

Fig. 3.4. Paleocurrent azimuthal patterns for the Ebenebe Sandstone at (a) Ugwuoba showing a bimodal pattern that is directed NW-SE and (b) at Ifite Awka.showing a bimodal pattern with a dominant mode that is directed southwest

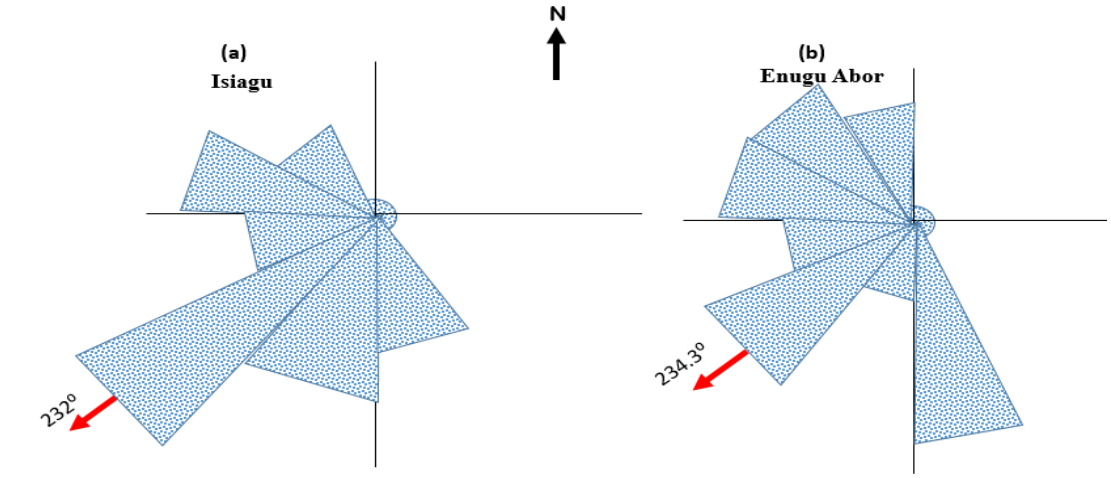

Fig. 3.5. Paleocurrent azimuthal patterns for the Ebenebe Sandstone at (a) Isiagu and (b) at Ifite Awka.showing a bimodal-perpendicular pattern in which the mean vector azimuth is directed south-westward.

At Ugwuoba the Ebenebe Sandstone exhibits a bimodal, paleocurrent azimuth pattern (Fig.3.4) that is directed NW-SE The mean vector azimuth is 314.22 º. Variance values is 14718, while the vector strength is 0.15 (Table 3.6) indicating a high dispersion of flow directions about the mean vector azimuth.

Table 3.6. Computational procedure for paleocurrent analysis at Ugwuoba

Ugwuoba	1 Azimuth (A)	2 Dip (D)	3 Sin A	4 Cos A	5 Cos D	6 5*4 (b)	7 5*3 (a)	8 Sin D (c)	9 $(A_1-314.2)^2$
1	304	22	-0.8290	+0.5592	+0.9272	+0.5184	-0.7686	0.3746	104.04
2	360	20	0.0	+1.0000	+0.9397	+0.9397	0	0.3420	2097.64
3	340	24	-0.3420	+0.9397	+0.9135	+0.8584	-0.3124	0.4067	665.64
4	330	19	-0.5000	+0.8660	+0.9455	+0.8188	-0.4727	0.3255	249.64
5	308	20	-0.7880	+0.6157	+0.9397	+0.5786	-0.7405	0.3420	38.44
6	340	23	-0.3420	+ 0.9397	+0.9205	+0.8650	-0.3148	0.3907	665.64
7	280	22	-0.9848	+0.1736	+0.9272	+0.1609	-0.9131	0.3746	1169.64
8	290	18	-0.9397	+0.3420	+0.9510	+0.3252	-0.8936	0.3090	585.64
9	300	21	-0.8660	+0.5000	+0.9336	+0.4668	-0.8085	0.3583	201.64
10	280	20	-0.9848	+0.1736	+0.9397	+0.1631	-0.9254	0.3420	1169.64
11	301	11	-0.8572	+0.5150	+0.9816	+0.5055	-0.8414	0.1908	174.24
12	300	14	-0.8660	+0.5000	+0.9703	+0.4851	-0.8402	0.2419	201.64
13	120	10	+0.8660	- 0.5000	+0.9848	-0.4924	+0.8528	0.1736	37713.64
14	129	13	+0.7771	-0.6293	+0.9744	-0.6132	+0.7572	0.2249	34299.04
15	145	18	+0.7071	-0.8191	+0. 9510	-0.7789	+0.6724	0.3090	28628.64
16	135	11	+0.7071	-0.7071	+0.9816	-0.6941	+0.6941	0.1908	32112.64
17	127	22	+0.7986	-0.6018	+0.9272	-0.5580	+0.7404	0.3746	35043.84
18	119	17	+0.8746	-0.4848	+0.9563	-0.4636	+0.8363	0.2924	38103.04
19	128	16	+0.7880	-0.6157	+0.9612	-0.5918	+0.7574	0.2756	34670.44
20	136	19	+0.6947	-0.7193	+0.9455	-0.6801	+0.6568	0.3255	31755.24
	TOTALS		-2.0863	2.0474		1.8134	-1.8638	6.1645	279650.00
	$(TOTALS)^2$		4.3526	4.1918		3.2884	3.4737	38.001	
Mean vector azimuth (*Arc tan R =(Σa) / (Σb)*:						R= $\tan^{-1}$ (-1.8638/1.8134). = -45.78º+360º=314.21º			
Variance Variance $S^2 = \Sigma (A_1-R)^2 / n-1$					:	S^2= 279650.00/19 = 14718			
Vector strength S= $\sqrt{(\Sigma sinA)^2+ (cosA)2 /n}$						S= $\sqrt{(4.3526+4.1918)/20}$ = 0.146			

ISSN No. 2321-2705 | DOI: 10.51244/IJRSI |Volume XII Issue VI June 2025

Table 3.7. Computational procedure for paleocurrent analysis at Ifite Awka

IFITE AWKA	1	2	3	4	5	6	7	8	9
Sample	Azimuth (A)	Dip (D)	Sine A	Cos A	Cos D	5*4 (b)	5*3 (a)	Sin D (c)	$(A_I\text{-}A)^2$
1	45	22	+0.7071	+0.7071	0.9272	+0.6556	+0.6556	0.3746	20061.8896
2	50	10	+0.7660	+0.6428	0.9848	+0.6330	+0.7543	0.1736	18670.4896
3	35	17	+0.5736	+0.8192	0.9563	+0.7834	+0.5485	0.2924	22994.6896
4	195	25	-0.2588	-0.9659	0.9063	-0.8754	-0.2345	0.4226	69.8896
5	185	19	-0.0872	-0.9962	0.9455	-0.9419	-0.0824	0.3255	2.6896
6	190	22	-0.1736	-0.9848	0.9272	-0.9131	-0.1609	0.3746	11.2896
7	190	17	-0.1736	-0.9848	0.9563	-0.9417	-0.1660	0.2924	11.2896
8	200	18	-0.3420	-0.9397	0.9510	-0.8936	-0.3252	0.3090	178.4896
9	198	16	-0.3090	-0.9511	0.9612	-0.9141	-0.2970	0.2756	129.0496
10	200	22	-0.3420	-0.9397	0.9272	-0.8713	-0.3171	0.3746	178.4896
11	180	11	0.0000	-1.000	0.9816	-0.9816	0.0000	0.1908	44.0896
12	185	14	-0.0872	-0.9962	0.9703	-0.9666	-0.0846	0.2419	2.6896
13	190	22	-0.1736	-0.9848	0.9272	-0.9131	-0.1609	0.3746	11.2896
14	205	18	-0.4226	-0.9063	0.9510	-0.8619	-0.4019	0.3090	337.0896
15	165	21	+0.2588	-0.9659	0.9336	-0.9017	+0.2416	0.3583	468.2896
16	180	10	0.0000	-1.0000	0.9848	-0.9848	0.0000	0.1736	44.0896
17	181	11	-0.0174	-0.9998	0.9816	-0.0981	-0.0171	0.1908	31.8096
18	135	16	+0.7071	-0.7071	0.9612	-0.6796	+0.6796	0.2756	2666.6896
19	292	11	-0.9272	+0.3746	0.9816	0.3677	-0.9101	0.1908	11100.7296
20	290	20	-0.9397	+0.3420	0.9397	0.3214	-0.8830	0.3420	10683.2896
	$\sum$		-1.2413	-11.4366		-9.9774	-1.1611	5.8623	87,698.3120
	$\sum^2$	2.57	1.5408	130.7958		99.5485	1.3481		
Mean vector azimuth (*Arc tan R =(Σa) / (Σb)*:					R= $\tan^{-1}$ (-1.1611/9.9774)=6.64°+180°=186.64°				
Variance Variance $S^2 = \Sigma (A_i\text{-}R)^2$ / n-1					S^2 = 87698.312/19=4615.70				
Vector strength S= $\sqrt{(\Sigma sinA)^2 + (cosA)^2}$ /n					*S*=√(1.5408) + (130.7959)/20 =0.57				

Table 3.8. Computational procedure for paleocurrent analysis at Isiagu

ISIAGU	1	2	3	4	5	6	7	8	9
Sample	Azimuth (A)	Dip (D)	Sine A	Cos A	Cos D	5*4 (b)	5*3 (a)	Sin D (c)	$(A_I\text{-}A)^2$
1	200	18	-0.3420	-0.9397	0.9510	-0.8936	-0.3252	0.3090	1197.1600
2	204	16	-0.4067	-0.9135	0.9612	-0.8780	-0.3909	0.2756	936.3600
3	181	12	- 0.0174	-0.9985	0.9781	-0.9766	-0.0170	0.2079	2872.9600
4	185	17	-0.0872	-0.9962	0.9563	-0.9526	-0.0834	0.2924	2460.1600
5	218	20	-0.6157	-0.7880	0.9397	-0.7404	-0.5786	0.3420	275.5600
6	208	16	-0. 4695	-0.8829	0.9612	-0.8486	-0.4513	0.5756	707.5600
7	213	15	-0.5446	-0.8387	0.9659	-0.8101	-0.5260	0.2588	466.5600
8	215	10	-0. 5736	-0.8191	0.9848	-0.8066	-0.5649	0.1736	384.1600
9	211	14	-0.5150	-0.8572	0.9702	-0.8316	-0.4996	0.2419	556.9600
10	212	13	-0.5299	-0.8480	0.9744	-0.8263	-0.5163	0.2249	510.7600
11	234	16	-0.8090	-0.5878	0.9612	-0.5650	-0.7776	0.2756	0.3600
12	232	16	-0.7880	-0.6157	0.9612	-0.5918	-0.7574	0.2756	6.7600
13	243	21	-0.8910	-0.4540	0.9336	-0.4238	-0.8318	0.3583	70.5600
14	247	20	-0.9205	-0.3907	0.9397	-0.3671	-0.8650	0.3420	153.7600
15	239	20	-0.8672	-0.5150	0.9397	-0.4839	-0.8150	0.3420	19.3600
16	296	15	-0.8988	+0.4384	0.9659	+0.4234	-0.8681	0.2588	3769.9600
17	301	11	-0.8572	+0.5150	0.9816	+0.5055	-0.8414	0.1908	4408.9600
18	298	15	-0.8829	+0.4695	0.9659	+0.4535	-0.8528	0.2588	4019.5600
19	313	19	-0.7314	+0.6820	0.9455	+0.6448	-0.6915	0.3255	6146.5600
20	290	16	-0.9397	+0.3420	0.9612	+0.3287	-0.9032	0.5756	3069.1600
	$\sum$		-12.6873	-9.881		-8.6401	-12.157	6.1047	32033.2000
	$\sum^2$	0.80	160.9676	97.6342					
Mean vector azimuth (*Arc tan R =(Σa) / (Σb)*:					R= $\tan^{-1}$ (-12.157/-8.6401)=54.60°+180°=234.60°				
Variance Variance $S^2 = \Sigma (A_i\text{-}R)^2$ / n-1					S^2 = 32033/19=1685.95				
Vector strength S= $\sqrt{(\Sigma sinA)^2 + (cosA)2}$ /n					*S*=√(97.6342+ (160.96/20 =0.80				

Table 3.9. Computational procedure for paleocurrent analysis at Ufuma

UFUMA	1	2	3	4	5	6	7	8	9
Sample	Azimuth (A)	Dip (D)	Sine A	Cos A	Cos D	5*4 (b)	5*3 (a)	Sin D (c)	$(A_I\text{-}A)^2$
1	160	10	0.3420	-0.9397	0.9848	-0.9254	+0.3376	0.1736	5641.5121
2	340	14	-0.3420	0.9397	0.9703	0.9118	-0.3318	0.2419	11001.9121
3	170	8	0.1736	-0.9848	0.9903	-0.9752	0.1719	0.1392	4239.3121
4	350	4	-0.1736	0.9848	0.9975	0.9823	-0.1732	0.0697	13199.7121
5	325	17	-0.5736	0.8191	0.9563	0.7833	-0.4698	0.2923	8080.2121
6	240	23	-0.8660	-0.5000	0.9205	-0.4602	-0.7971	0.3907	23.9121
7	310	20	-0.7660	0.6428	0.9397	0.6040	-0.7198	0.3420	5608.5121
8	230	15	-0.7660	-0.6428	0.9659	-0.6207	-0.7399	0.2588	26.1121
9	245	20	-0.9063	-0.4226	0.9397	-0.3971	-0.8516	0.3420	97.8121
10	210	10	-0.5000	-0.8660	0.9848	-0.8528	-0.4924	0.1736	630.5121
11	160	22	0.3420	-0.9397	0.9272	-0.8713	+0.3171	0.3746	5641.5121
12	225	18	-0.7071	-0.7071	0.9510	-0.6724	-0.6724	0.3090	102.2121
13	240	17	-0.8660	-0.5000	0.9563	-0.4781	-0.8281	0.2923	23.9121
14	242	15	-0.8829	-0.4695	0.9659	-0.4535	-0.8528	0.2588	47.4721
15	280	20	-0.9848	0.1736	0.9397	0.1616	-0.9254	0.3420	2015.1121
16	301	11	-0.8572	0.5150	0.9816	0.5055	-0.8414	0.1908	4341.4921
17	300	14	-0.8660	0.5000	0.9703	0.4851	-0.8428	0.2419	4210.7121
18	165	15	0.2588	-0.9659	0.9659	-0.9330	0.2500	0.2588	4915.4121
19	155	10	0.4226	-0.9063	0.9848	-0.8925	0.4162	0.1736	6417.6121
20	169	13	0.1908	-0.9816	0.9743	-0.9564	0.1859	0.2249	4370.5321
21	227	15	-0.7313	-0.6819	0.9659	-0.6586	-0.7063	0.2588	65.7721
22	231	14	-0.7771	-0.6293	0.9703	-0.6106	-0.7540	0.2419	16.8921
$\sum$			-9.1467	-6.5622		-6.3242	-9.0703		80718.1362
$\sum^2$		0.511	83.6621	43.0625					
Mean vector azimuth (*Arc tan R =(Σa) / (Σb)*:					R= $\tan^{-1}$ (-9.0703/-6.3242)=55.1141°+180°=235.11°				
Variance Variance $S^2 = \Sigma (A_i\text{-}R)^2$ / n-1					S^2 = 80718/21=3843.72				
Vector strength S= $\sqrt{(\Sigma sinA)^2 + (cosA)2}$ /n					*S*=√(83.6621+ (43.0625/22 =0.51				

ISSN No. 2321-2705 | DOI: 10.51244/IJRSI |Volume XII Issue VI June 2025

- At Ifite Awka the Ebenebe Sandstone exhibits a bimodal, palaeocurrent azimuth pattern (Fig.3.4) with a dominant mode that is directed southwest-ward The variance is 4615 and the vector strength is 0.57 (Table 3.7), also indicating a high dispersion of flow directions about the mean vector azimuth.

Table 3.10. Summary of the interpretation of the paleocurrent patterns of the Ebenebe Sandstone in the study area.

Locality	Pattern	MVA	Variance	Vector Strength	Depositional Interpretation
Ugwuoba	Bimodal	314.22º	14718	0.15	Deltaic
Ifite Awka	Bipolar perpendicular	186.64º	4615.7006	0.57	Deltaic
Isiagu	Fan shaped/bimodal-perpendicular	234.60º	1685.9579	0.80	Deltaic
Enugu Abor	Fan shaped/bimodal-perpendicular	235.11	3843.7207	0.51	Deltaic

- The pattern at Isiagu and Enuuabor-Ufuma is essentially perpendicular-bimodal and radiating (Fig.3.5). Mean vector azimuth averages 235º, while the variance ranges between 1686 and 3844). Dispersion of flow directions about the mean vector azimuth fluctuates between 0.5 and 0.8 (Tables 3.8 & 3.9).

- By comparison with the shoreline paleocurrent models of Selley (1968)[35], the Ebenebe Sandstone is interpreted to be a fluvio-deltaic deposit that accumulated along a shoreline in which fluviatile currents (the southwest mode) were present with net along-shore (the SE-NW mode) marine transport (Fig. 3.6).

- The Ebenebe Sandstone is therefore envisaged to be derived from an easterly source region, transported to the depositional site by a southwesterly fluvial currents and re-distributed by the SE-NW marine currents to form the Ebenebe Sandstone ridge.

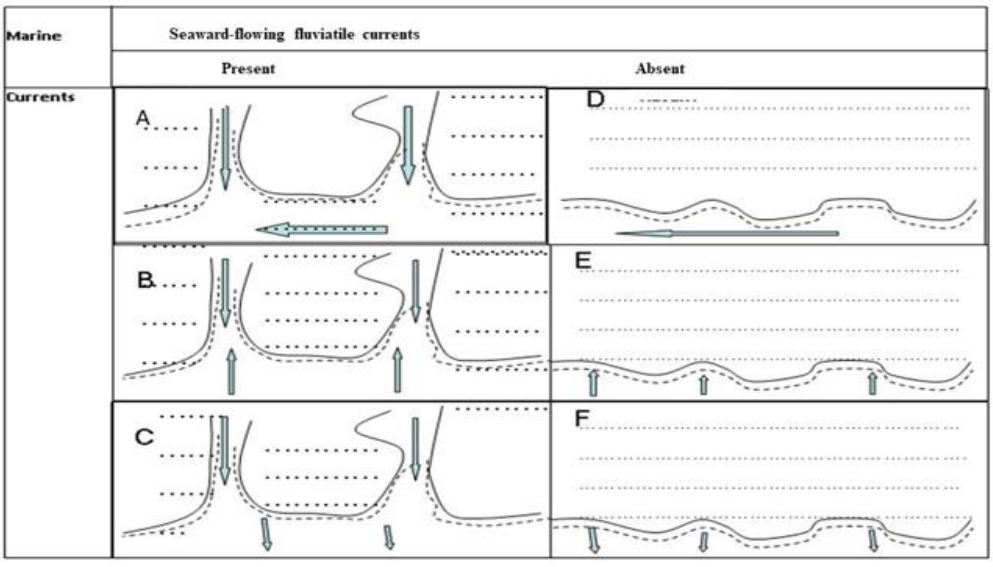

Fig. 3.5. Shoreline paleocurrent model (Selley, 1968)[35] showing seaward (southward) flowing fluvial currents, landward (northward) flowing tidal currents and horizontal (east-west) flowing longshore flowing currents

DISCUSSION AND CONCLUSIONS

Discussion

Results of provenance studies of the sandstones of the Anambra and Niger delta basins (e.g., Hoque, 1977[36]; Amajor, 1987[37], Hoque & Nwajide, 1985[12], Obi, 2000[16]) have established that the provenance of the Maastrichtian-Eocene formations in the Anambra Basin is a mix of sediment sources, including the Oban

Massif, the West African Massif, and recycled sedimentary rocks from the Anambra Basin and Afikpo Syncline. According to Obi *et al,* (2001)[6], the Anambra Basin which was formed following the Santonian tectonic upheaval in the Benue Trough, continued to subside asymmetrically as Campanian-Eocene sedimentation progressed in the basin. An episode of strong subsidence occurred in the southern part of the Anambra platform about the Danian period, uplifting the proximal flank of the basin and dislocating the depocentre further southward to the Niger Delta. Consequently the uplifted western flanks of the Anambra basin composed of Maastrichtian sedimentary rocks served as the dispersal centre from which pre-Paleocene sediments were eroded and transported into the Niger Delta (Obi et al., 2001)[6]. Results of the present study are consistent with the above interpretations.

This study has shown that the Ebenebe Sandstone is a quartz arenite that was recycled from a pre-existing sedimentary terrain and deposited as a fluvio-deltaic deposit. The occurrence of bimodal and bipolar, often radiating palaeocurrent azimuthal patterns in the Ebenebe sandstones, is recognized as a reliable signature of deltaic sedimentation. Bimodal palaeocurrent systems with bipolar modes are common in settings where tidal processes are significant (Selley, 1968[35]; Kreisa and Moiola 1986[38]; Dalyrimple, 1992[39]). In such settings the bipolar pattern defines the axis of the alternating ebb and flood currents that prevailed during the deposition of the sediment, the stronger current representing the flood stage (Dalyrimple 1992)[39]. In the present work, the bipolar pattern exhibited by the Ebenebe Sandstones coincides with the axis of the alternating seaward directed fluvial currents, and the landward directed ocean currents. The southerly directed components of the mutually opposed azimuthal patterns exhibited by the sandstones (Figs. 3.4. & 3.5) may also be attributed to seaward directed fluvial flows emanating from the pre-Paleocene provenance regions including the emergent Campanian-Maastricthian strata of the Anambra Basin.

Conclusions

1. Results of this investigation has revealed that Ebenebe Sandstone contains up to 90% Quartz (SiO_2) and subordinate average amounts of Alumina, Al_2O_3, (5.30%), and Iron oxide, Fe_2O_3 (23.20%). The observed high average ratio of SiO_2 to Al_2O_3 in the samples indicates that the Ebenebe Sandstones in the study area contains minimal clay or detrital Aluminum silicate.
2. The low percentage of total alkali-earth oxides suggests that the Ebenebe Sandstone is dominantly cemented by silica.
3. Based on the log ratios of chemical oxides and on the classification scheme of Pettijohn (1975)[40], the Ebenebe Sandstone is classified as silica-cemented quartz arenite.
4. Evidence from chemical indices and the Rose diagrams indicates that the Ebenebe Sandstone was generated from a pre-existing sedimentary terrain located to the northeast of the present study area. The terrain experienced intense chemical weathering. The geological map of south-eastern Nigeria (Nwajide, 2013)[2] shows that this region is underlain by the Maastrichtian strata which according to existing literature, progressively became emergent as a result of the asymmetrical subsidence of the post-Santonian Anambra basin.
5. Consequently the uplifted western flanks of the Anambra basin composed of Maastrichtian sedimentary rocks served as the dispersal centre from where pre-Paleocene sediments were eroded and transported by southwest-flowing fluvial currents into the Niger Delta (Obi et al., 2001)[6] to form a linear sand ridge called the Ebenebe Sandstone.
6. These results thus provide new insight into the paleo-geographic history of the Anambra-Niger delta basin complex.

ACKNOWLEDGEMENTS

This study was funded by the Obinenwu Foundation and TETFUND. We are grateful to Prof (Mrs) Shirley Odunze-Akasiugwu and an anonymous reviewer for their thorough and thoughtful reviews of the manuscript.

REFERENCES

1. Ezeani, U.S. (2025). Depositional Model and Silica Sand Potential of the Ebenebe Sandstone Ridge, Anambra State. PhD. Thesis. Chukwuemeka Odumegwu Ojukwu University, Anambra State, Nigeria.

2. Nwajide, C.S. (2013). Geology of Nigerians Sedimentary Basins; CSS Bookshops Limited, 565.
3. Odunze, S.O. & Obi, G.C. (2014). Sedimentology and Sequence Stratigraphy of the Nkporo Group (Campanian-Maastrichtian), Anambra Basin, Nigeria. Journal of Paleogeography, 2(2): 192-208.
4. Ekwenye, O.C., Nichols, G.J., Collinson, M., Nwajide, C.S., & Obi, G.C. (2014). A Paleogeographic Model for the Sandstone Members of the Imo Shale, South Eastern Nigeria. Journal of African Earth Sciences 96, 190 – 211.
5. Ohwona O. C & Okoro, A.U. 2022. Depositional facies analysis of the Ebenebe Sandstone outcropping in Ugwuoba, Umuogbuefi-Ebenebe and Isiagu area of the southeastern Nigeria. Global Scientific Journal 10 (3), 7-29.
6. Obi, G.C., Okogbue, C.O. & Nwajide, C.S. (2001). Evolution of the Enugu Cuesta: A tectonically driven erosional process: Global Journal of Pure & Applied Sciences, 7, 321–330.
7. Fairchild, I.J, Hendry G, Quest, M., and Tucker, M., (1988). Chemical analysis of sedimentary rocks. In: Techniques in Sedimentology (Ed. by Tucker, M), pp. 274-354. Blackwell Scientific Publications.
8. Reyment, R.A. (1965). Aspects of the Geology of Nigeria: University of Ibadan Press, Nigeria.
9. Burke, K., (1996). The African Plate. South African Journal Geology, 99, 341-409.
10. Murat, R. C. (1972). Stratigraphy and palaeogeography of the Cretaceous and Lower Tertiary in southern Nigeria. In: T. F. J. Dessauvagie and A. J. Whiteman (eds.), African Geology, Univ. of Ibadan Press, Nigeria. 251-266.
11. Benkhelil, J. (1989). The origin and evolution of the Cretaceous Benue trough (Nigeria). African Earth Science, 8: 251-282.
12. Hoque, M. & Nwajide, C.S., (1985). Tectono-sedimentological evolution of an elongate Intracratonic basin (Aulacogen): The case of the Benue Trough of Nigeria. Nigerian Journal of Mining and Geology, 21(1&2), 19-26.
13. Ojoh, K.A. (1992). The southern part of the Benue Trough (Nigeria) cretaceous Stratigraphy, Basin Analysis, Paleo-oceanography and Geodynamic Evolution in the Equatorial domain of the South Atlantic. NAPE Bull 7: 131-152.
14. Popoff, M. (1990). Deformation intracontinental gondwanienne-Rifting Mesozoique en Afrique (Evolution Meso-Cenozoique du fosse de la Benue, Nigeria)-Relations de li ocean Atlantique sud. These de Etat, University Aix- Marseilla III.
15. Binks, R. M. and Fairhead, J. D. (1992). A plate tectonic setting for Mesozoic rifts of West and Central Africa. Tectonophysics. 213, 141-151.
16. Obi, G.C. (2000). Depositional Model for the Campanian-Maastrichtian Anambra Basin, Southeastern Nigeria. PhD Thesis, Dept. of Geology, University of Nigeria, Nsukka.
17. Oboh-Ikuenobe, F.E., Obi, G.C., & Jaramillo, C.A. (2005). Lithofacies, palynofacies and sequence stratigraphy of Paleogene strata in southeastern Nigeria; Journal of African Sciences, 41, 75-100.
18. Odunze-Akasiugwu, O. S. & Obi, G.C. (2019). The Ameke Abam-Ebenebe Sand Ridge, Southeastern Nigeria: A Fluvio-deltaic Deposit. Oriental Journal of Science and Engineering, 1(1), 1-12.
19. Steinmetz, R. (1962). Analysis of vectorial data: Journal of Sedimentary Petrology, 32, 801-812.
20. Marsal, D. (1987). Statistics for Geoscientists. Pergamon Press, Oxford, London.
21. Collinson, J.D. &Thompson, D.B. (1989). Sedimentary Structures: Chapman and Hall, London.
22. Nesbitt, H.W., Young, G.M., McLennan, S.M., & Keays, R.R. (1996). Effect of chemical weathering and sorting on the petrogenesis of siliciclastic sediments, with implications for provenance studies. Journal of Geology. 104, 525–542.
23. Pettijohn, F.J., (1963). Chemical composition os Sandstone – excluding carbonateand volcanic sands. In: Data of Geochemistry (6th Ed.). U.S. Geol. Survey Prof. Paper 440S, 19p.
24. Pettijohn, F.J., Potter, P.E., and Siever, R. (1972). Sand and Sandstone. New York, Springer Verlag, 618p.
25. Herron, M.M. (1988). Geochemical classification of terrigenous sands and shales from core or log data. Journal of Sedimentary Petrology, 58, 820-829.
26. Roser, B.P., & Korsch, R.J. (1988). Provenance signatures of sandstone-mudstone suites determined using discriminant function analysis of major-element data: Chemical Geology, 67, 119-139.
27. Crook, K. A. W. 1974. Lithogenesis and geotectonics: the significanse of compositional variations in flysch arenites (graywackes). *In: Dott, R. H. &* Shaver, R. H. (eds) Modern *and ancient geosynclinals*

sedimentation. Society of Economic Paleontologists amf Mineralogist Special -Publication, 19, 304-310.

28. Nesbitt, H.W., Young, G.M. (1982). Early Proterozoic climates and plate motions inferred from major element chemistry of lutites. Nature 299, 715-717.
29. Elzien, S.M., Farah, A. A., Alhaj, A. B., Mohamed, A.A., Al-Imam, O.A.O., Hussein, A. H., Khalid, M. K., Hamed, B.O., & Alhaj, A. B. (2014). Geochemistry of Merkhiyat Sandstones, Omdurman Formation, Sudan: Implication of depositional environment, provenance and tectonic setting. International Journal of Geology, Agriculture and Environmental Sciences. 2, (3), 10-15.
30. Mgbenu, C.N, 2018. Sedimentology and economic potentials of sandstones in the Amaokpala-Awka area of Anambra State, south-eastern Nigeria. MSc Dissertation. Chukwuemeka Odumegwu Ojukwu University, Anambra State, Nigeria.
31. Echefu, K.I. (2019). Sedimentology and economic potential of sandstones in the Nando-Obosi area of Anambra State, southeastern Nigeria. MSc. Dissertation. Chukwuemeka Odumegwu Ojukwu University, Anambra State, Nigeria.
32. Fedo, C.M., Nesbitt H.W. & Young, G.M. (1995). Unraveling the effects of potassium metasomatism in sedimentary rocks and paleosols, with implications for paleoweathering condiions and provanence. Geology 23, 10, 921-924.
33. Dupuis, C, Hebert, R, and Cote, V.D. (2006). Geochemistry of sedimentary rocks melange and flysch units south of the Yarlung Zangbo suture zone, southern Tibet. Journal of Asian Earth Sciences, 26, 489-508.
34. Harnois,L. (1988). The C.I.W. index: a new chemical index of weathering. Sedimentary Geology 55, 319-322.
35. Selley, R. C., (1968). A classification of paleocurrent models. Journal of Geology, 76, 99-110.
36. Hoque, M., 1977. Petrographic differentiation of tectonically controlled Cretaceous sedimentary cycles, southeastern Nigeria. Sediment. Geol., 17, 235-245.
37. Amajor, L. C., 1987. Paleocurrent, petrography and provenance analyses of the Ajalli Sandstone (Upper Cretaceous), Southeastern Benue Trough, Nigeria, Sediment. Geol., 54, 47-60.
38. Kreisa, R. D., and Moiola, R. J., 1986. Sigmoidal tidal bundles and other tide-generated sedimentary structures of the Curtis Formation. Utah. Geol. Soc. Amer. Bull., 97, 381-387.
39. Dalrymple, R. W., 1992. Tidal depositional systems, in Walker, R. G., and James, N. P. (eds.). Facies Models: Response to sea level changes: Geological Association of Canada, p. 195-218.
40. Pettijohn, F. J. 1975. Sedimentary rocks 3rd ed. New York. Harper and Row.